AN EXPERIMENTAL STUDY ON NONLINEAR WAVE DYNAMICS: ROUGE WAVE GENERATION AND WAVE BLOCKING

Wen-Yang Hsu[1], Igor Shugan[1], Wen-Son Chiang[1], Ray-Yeng Yang[1], Hwung-Hweng Hwung[2], Sergey Kuznetsov[3] and Yana Saprykina[3]

Wave modulation due to Bengamin Feir Instability (BFI) in the presence of long wave (swell) is investigated in the elaborate experiments. The mechanically generated waves are composed of three discrete waves; while the newly generated harmonics due to BFI still combining into discrete spectra with the same frequency difference step. These stable discrete waves allow us to further examine the basic properties of nonlinear wave-wave interactions, such as the variation of phase speeds and wave numbers along the wave tank together with speed of crests, especial for the large transient waves. The measured values have a reasonable correspondence to the available nonlinear model estimations. The technique proposed in this study is verified to accurately measure the phase speed and wave number of each harmonic in the wave group. Phase speeds of short waves have a significant amplification in the vicinity of big transient waves, while the speeds of longer waves are close to linear values. The relative long wave (storm wave) travelling with short waves (wind waves) dramatically change the local kurtosis and skewness and may have an important role for the generation of large transient wave and provide an opportunity for triggering the freak waves.

Keywords: Benjamin Feir Instability, giant wave, phase speed, nonlinear wave

INTRODUCTION

The random sea exhibits nonlinear water wave group behavior. The modulational instability has been considered one of the key processes to determine the nonlinear energy transfers and wave breakings in the deep water (Benjamin and Feir 1967). Owing to the difficulties of characterizing the modulational instability in the open sea, there is a widespread laboratory experiments which simplified the real sea state as several discrete waves. Many researches focused on the evolution of wave modulation and have found some remarkable results, such as recurrence without downshifting (Fermi-Pasta-Ulam recurrence), temporal and permanent wave energy peak downshifting, accompanied by the wave breaking (Tulin and Waseda 1999; Hwung-Hweng Hwung et al. 2011), the initial wave steepness value for breaking criteria (Tulin and Waseda, 1999; Chiang and Hwung, 2007, Hwung et al. 2007; Galchenko et al. 2010; Banner 2014) and wave cascade generation by Kartashova & Shugan (2011). Furthermore, Benjamin-Feir instability on its further stages up to breaking is intensely studied, been suggested to be one of basic mechanisms of freak wave formation (Kharif and Pelinovsky 2003).

The principal parameter which influences the growth rate of sidebands and breaking criteria is the wave steepness. From the temporal and spatial evolution of a group wave it is not straightforward to define the wavenumber at any arbitrary position. As a result, different definitions of wavenumber are proposed to study the wave of interest. For example, Melville (1983) applied the Hilbert transform to define the instantaneous frequency and amplitude for a train of modulated wave evolving in space and time. His results found that the local frequencies are highly phase dependent and sometimes go to zero or even negative when the phase reversals occurred. On the other hand, the measurement of time between crests or zero-crossing points associated with the wave of interest are commonly adopted to measure the local phase speed, wavenumber and wave steepness (Stansell and MacFarlane 2002; Grue et al. 2003). Many results obtained from the above definitions focus on the characteristics of most energetic wave (e.g., breaking wave), which is treated as an individual wave and described by a single parameter (e.g., phase speed). Nevertheless, the giant wave formation may appear due to the spatial wave focusing (geometrical focusing) and spatio-temporal focusing (dispersion enhancement), where various independent harmonic waves propagating with their own phase speeds (Kharif and Pelinovsky 2003).

Nonlinear behavior of waves exhibit itself beside the changing of amplitudes and spectral structure of the wave packet in significant variations of kinematic characteristics for every wave component such as phase speed, local wave number etc. There exist some confusion and gap concerning this issue in the literature, where the wavenumber in the wave group is often studied for individual wave without

[1] International Wave Dynamics Research Center /Tainan Hydraulics Laboratory, National Cheng Kung University, 5th F., No. 500, Sec. 3, Anming Rd., Tainan, 709, Taiwan
[2] Department of Hydraulics and Ocean Engineering, National Cheng Kung University, No.1 University Rd., Tainan, 701, Taiwan
[3] Institute of Oceanology of Russian Academy of Science, Vavilova 38, Moscow, Russia

considering the intrinsic waves. It is interesting to study the nonlinear variation of wave number and phase speed for every harmonic in the wave train along the long fetch and to compare the results with the available linear and nonlinear modeling approaches.

Moreover, the quasi-resonant interaction between free modes may result in an increase (in deep water) of kurtosis with respect to its Gaussian value, which is described by a four-wave interaction developed by Janssen (2003). The modulational instability process in the ocean due to wind waves and long swells has been recognized to be responsible for a fishing boat that was mysteriously sank off the east coast of Japan (Tamura 2009). Nevertheless, few laboratory experiments investigated the evolution of large transient waves by considering the interaction of short and long waves. In the present study, we will generate the nonlinear wave train with long and short waves together and evaluate the occurrence of extreme waves under Bengimin-Feir instability.

LABORATORY EXPERIMENTS

The experiments were conducted in the wave flume at Tainan Hydraulics Laboratory. The flume is 200 m long, 2 m wide and 2 m deep (see Fig.1 for the detail setup). A piston-type wavemaker with programmable function is equipped at the one end of the wave flume. In the following, we set x=0 m at the mean position of wave paddle. In order to observe the wave deformation in a uniform water depth, the surface wave will be measured before the trapezoid bar (x=67~117 m). Twelve capacitance-type wave gauges were used to measure the spatial and temporal evolution of the surface waves with a sampling rate 50Hz. Starting from the third wave gauge, the wave gauges are placed with an equal spacing of 4 m. Each experimental run was recorded for 10 min in real time, including the initial ramp-up. For the present experiments the water depth was fixed at 1.3 m. Three scenarios of group wave were mechanically generated according to the specified wave form:

$$\eta(t) = a_c \cos(2\pi f_c) + a_- \cos(2\pi f_-) + a_s \cos(2\pi f_s) \qquad (1)$$

Table 1. Test conditions and the corresponding wave properties

	$f_c\ (Hz)$	$f_s\ (Hz)$	a_- / a_c (a_c=0.07 m)	a_s / a_c	$\varepsilon = k_c a_c$	$k_c h$	$\frac{\Delta\omega}{\omega_c / \varepsilon}$
Case 1	0.84	0.56	0.1	0.4	0.19	3.7	0.77
Case 2	0.84	NA	0.1	NA	0.19	3.7	0.77
Case 3	0.84	NA	NA	NA	0.26	3.7	NA

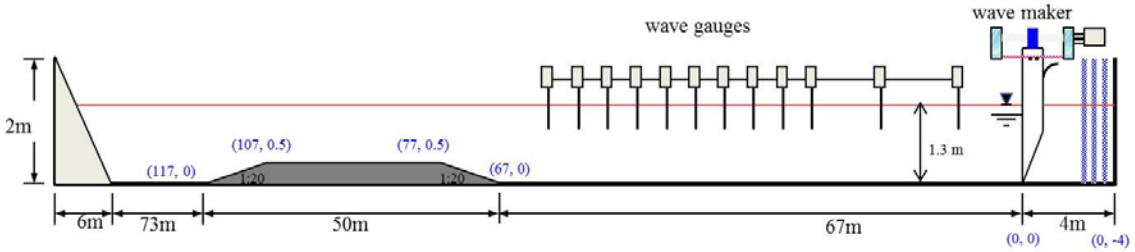

Figure 1 (a) Schematic view of the experimental setup.

EXPERIMENTAL RESULTS

Surface Elevation and Basic Property

The initial wave steepness,ε, for Case 1 is 0.19 and the relative water depth is in the deep water condition (kh= 3.70). The spatial evolution of the surface elevation and Fourier amplitudes as a function of fetch are shown in Fig. 2 and Fig 3. In the initial stage (kx <23), the modulational characteristics of the "seeded" sub-harmonic created a symmetric super-harmonic at f+=0.98 Hz. As a result, the initial group wave can be treated as a linear superposition of one carrier wave and two small sidebands together with a low frequency wave. After, the group wave train exhibits a slow oscillation with an increasing trend that accompanies the symmetric growth of the sidebands until kx=88. As the wave train further evolves, asymmetric growth of the sideband amplitudes is observed after kx=122, where some occasional small wave breakings appear in the experiment. This confirms that the initiation of asymmetric development of sideband amplitudes after initially exponential growth roughly corresponds

to the onset of wave breaking on a strongly modulated wave train (e.g., Melville 1983; Chiang and Hwung 2007).

Then, the modulation of the wave train increases until the strongest modulation is reached at kx=168, where most of the energy of the wave train is focused into the wave group center with four energetic individual waves. Moreover, we observe a sequence of large transient waves and the peak wave heights are around 0.33 m (about 1.8 times significant wave heights under the definition of Hs=4σ). The result reveals a mechanism for the generation of a freak wave resulting from sideband instability. These features will be analyzed in more detail later in Sec. 3.3 and 3.4. Around this stage, strong wave breaking is identified on the front of the modulated wave train according to a video record of the experiment.

The initial wave train in the Case 1 is mechanically generated by three discrete waves, while more than eight discrete waves are observed at the final wave gauge. All the newly generated harmonics have the same seeded frequency difference (0.14 Hz), and they are produced by the quasi resonance nonlinear wave interactions such as BFI and self interactions of the higher order Stokes waves. These discrete set of waves in this study allow us to further examine the variation of phase speed of each harmonic, especial for the large transient wave. The analysis technique will be presented in the next section.

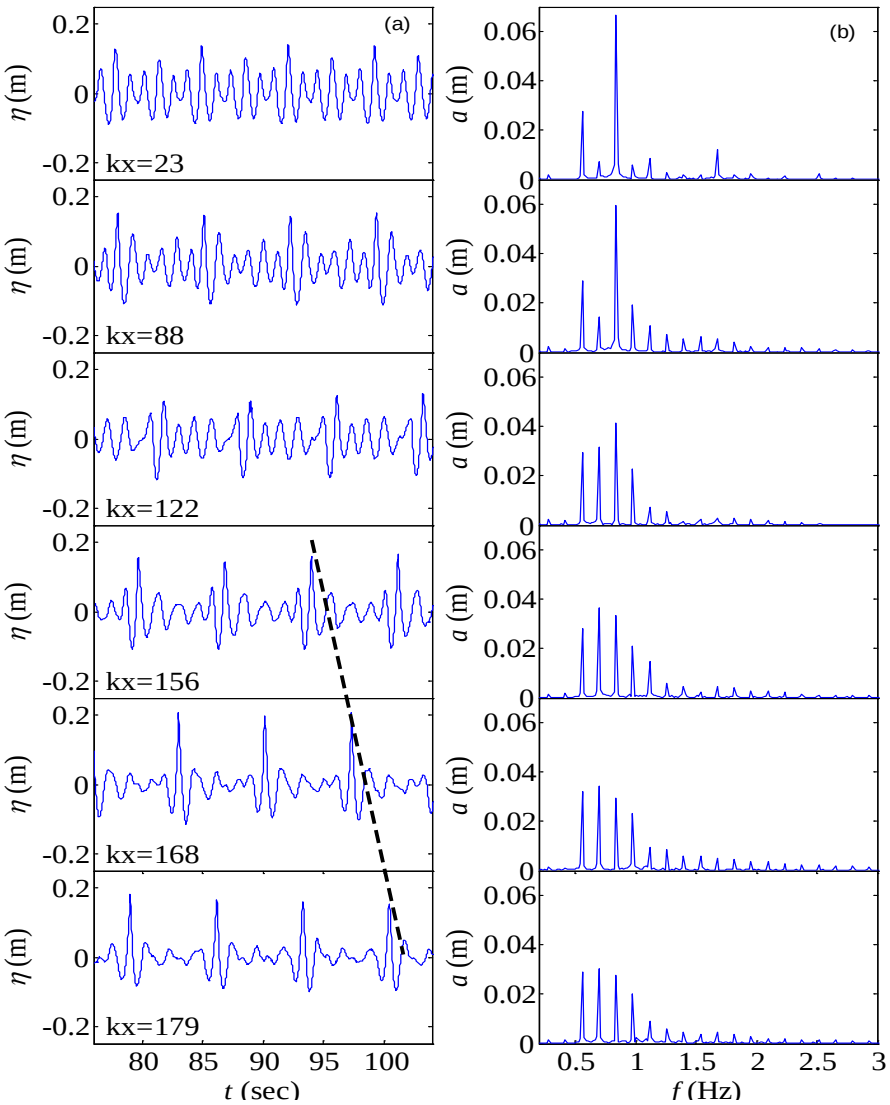

Figure 2. (a) The measured surface elevations at several selected locations.(b) The corresponding Fourier amplitudes. The dashed line indicates the local maximum elevation and they are used to calculate the wave speed in Sec. 3.4.

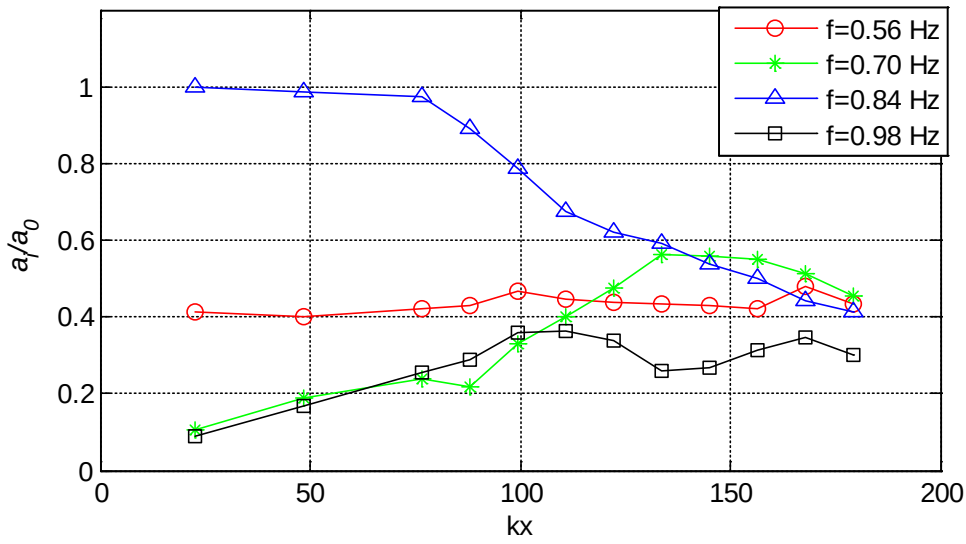

Figure 3. The spatial evolution of dimensionless amplitudes

Measurement of phase speed

The Fast Fourier Transform (FFT) is widely used for water wave problems, especially in the frequency spectral evolution of wave groups. In this study, the FFT is used to calculate the phase speed of individual harmonic via two adjacent wave gauges. The traditional approach that traces the time of crest/crossing point from the neighboring wave gauges has been successfully applied by Lake and Yue (1978). Their results showed that the phase speeds of high order bands in the Stokes wave are bounded to the main frequency wave. Based on their results, though the FFT is a linear processing method, it still can estimate the nonlinear phase speed within the framework of Stokes wave.

It is expected that the crest-tracing approach may fail for the continuous spectra wave because the local crests in the group wave are usually the superposition of several harmonics. However, for a stationary and discrete frequency wave spectrum, such as carrier wave travel with sidebands, the FFT method can effectively separate the group wave into individual harmonics and provide their amplitudes and phases. As a result, the crest tracing approach can be applied to the re-constructed time series of the surface elevation for single harmonic. The time series of surface wave at any point can be written as the superposition of several harmonics:

$$\eta(x,t)=\sum_{i=1}^{N} a_i \cos(\omega_i t - k_i x + \phi_i) \qquad (1)$$

where a is amplitude, ω is angular frequency, k is wavenumber and ∅ is phase. In the FFT analysis, the surface elevation at each wave gauge is:

$$\eta(t)=\sum_{i=1}^{N} a_i \cos(\omega_i t + \phi_{iFourier}) \qquad (2)$$

where the $\phi_{iFourier}$ is Fourier phase of each component. The FFT yields the phase relative to the start of the time-domain signal. If we select the same start time in the FFT analysis for all wave gauges, the $\phi_{Fourier}$ also represents the quantity of $-kx+\phi$. As a result, the Fourier phase difference between two adjacent wave gauges is mainly contributed by the $k\Delta x$, in which the variation of ∅ within a short distance is small and is assumed to be zero here. The space-average wavenumber and the phase speed can be obtained. It is noted that the phase from FFT generally has big confidence intervals because the degree of freedom are low. In order to minimize the instability and evaluate the repeatability of signal, we employ the multi-taper method. It separates the signal into several segments and then output their mean value via ensemble average.

To verify this method, the Case 3 (monotonic Stokes wave with ε=0.26)) is selected as an example to compare the calculated phase speed from FFT algorithm along with the linear and 3rd Stokes solution. Figure 4 shows the phase speeds obtained from different approaches and all results are normalized by the linear solution. The measured phase speed shows a typical result of Stokes wave that

is close to the 3rd Stokes solution. Importantly, the good agreement (< 1% difference) indicates that the FFT approach can be used to describe the phase speed evolution of Stokes wave. Finally, the standard deviation is computed as an indicator of the wave repeatability and uncertainty from gauge spacing, frequency resolution. (see the error bars in Figures 4).

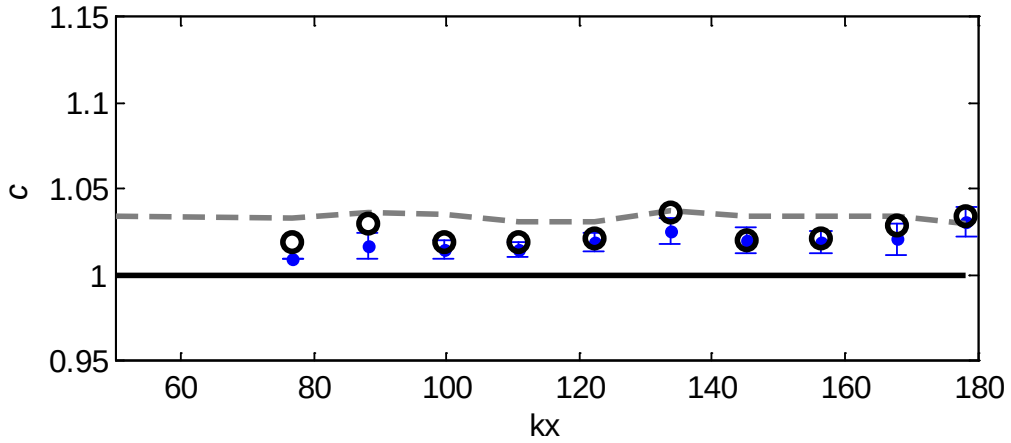

Figure 4. The spatial evolution of nondimensional phase speed for Case 3. Solid line: linear solution; dashed line: 3rd Stokes solution; circles: crossing point method; solid points: FFT method

Results of group wave

Similar to the Case 3, the spatial distribution of phase speed for each harmonic was calculated, as shown in the Figure 5 and compare it with the theoretical estimations by the linear, nonlinear 3rd order Stokes solution and multi-resonant model following from the dispersion relations for every harmonic (Phillips 1977):

$$\sigma_i^2 = gk_i\left(1+\sum Q_{ij}a_j^2k_j^2\right) \qquad (3)$$

where Q_{ij} are coefficients of nonlinear Stokes dispersion for the multi-resonant system. The measured phase speed for the low frequency wave remains stable and is predicted well by the linear solution. For the carrier wave, the phase speed generally exhibits an acceleration process, while the sidebands show several oscillations. It is interesting to note that higher frequency wave has a larger discrepancy from the linear solution, which indicates the nonlinearity (e.g., steepness) is an important factor. Moreover, the faster nonlinear phase speed corresponds to the increased steepness and they maximally approaches to 1.1 times of the linear wave speed (Longuet-Higgins 1975). We also note that at *kx*~170 all the phase speeds accelerate until the large transient wave occurred. The increasing phase speeds are mainly occurred around *kx*~100 and *kx*~170, where the two wave breaking events are observed. In general, the measurements are not described well either by the 3rd order Stokes solution or multi-resonant solution. The strong nonlinearity and energy dissipation is considered as the main reason and that should be further studied.

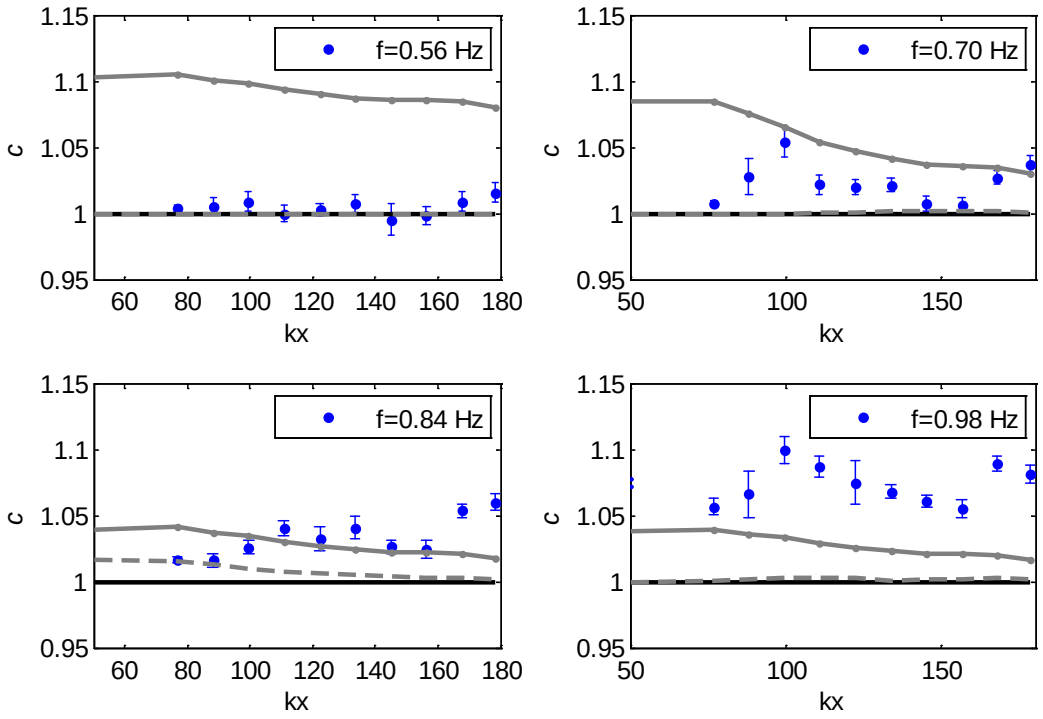

Figure 5. The spatial evolution of nondimensional phase speed for Case 1. Solid line: linear solution; dashed line: 3rd Stokes solution; circles: crossing point method; solid points: FFT method; gray line: the resonant solution

Large Transient waves

In this section the generation of large transient waves in the Case 1 is discussed. The carrier wave with sidebands evolves to three focused energy waves due to BFI. In the meanwhile, the low frequency wave mostly remains its amplitude all along the wave flume and hence it is interesting to note that the four-wave system with equal amplitude is observed around *kx*=168. At this position, the time series of the superposition of four decomposed harmonics plotted with the measured data and individual harmonic are also presented, as shown in the Fig. 6. All harmonic waves (the others not shown) come into the same phase at the maximum elevations. The crest of giant wave is formed by the superposition of Fourier harmonics (marked as dash lines), while the zero elevation is caused by the neutralization of local crests and troughs (e.g., at t= 7.6 sec). Additionally, the wave is traveling inside an envelope with a period *Tp*, which is equal to the frequency difference (e.g., $Tp=1/\Delta f$).

The reference Case 2 is a typical BFI scenario and the ratio of the maximum wave height to the significant wave height is only 1.4, where there are no giant waves is observed. As a result, the long wave effect is examined by comparing with Case 2, as shown in the Figure 7a. Although the long wave changes the whole wave structure, however, the growth rate and energy transfers between carrier and sidebands are not greatly enhanced. The long wave increases the local steepness and hence changes the breaking criteria. The maximum discrepancies are observed at the sub-harmonic near the back-end, where the wave breaking occurred in the Case 1.The position of the main wave breakings of Case 1 is around 15 m downstream to the Case 2. However, it is interesting to note that the kurtosis of the surface elevation along the fetch is greatly different for Case 1 and Case2. The maximum of the kurtosis takes a place around *x*= 60 m and it corresponding to the position of giant wave occurrence, as shown in Fig 7b. The relative long wave (storm wave) travelling with short waves (wind waves) dramatically change the local kurtosis and may play an important role for the generation of large transient waves and can provide an opportunity for triggering of the freak waves.

A series of giant wave was identified from the last three measurements (tracing the maximum surface elevation starting from *kx*=156, 168 to 179, see the dash line in Fig.2). Following the definition of phase speed by tracing the crest from adjacent wave gauges, it gives an average group speed of 1.21 and 1.19 m/s. Figure 8 shows the 3-D surface elevation between *kx*=156 and 168 in the space and time

domain. This plot is generated from Eq. (1) by taking linear interpolation of the measured amplitudes and wavenumbers and neglecting the change of the "initial" phase. The maximum surface elevation at *kx*=156 and 168 is marked as number 1 and 4. It is can be found that the giant wave does not come from point 1, but grow from a small wave (point 3) and with a phase speed of 2.1 m/s. By tracing the point 1 to 4, it gives the same speed as the result from the Fig.2and which represents the group speed. The phase speed of giant wave is around two times of group speed and relatively higher than the surrounding waves. Live time of giant wave is relatively short and that is why, probably, there is no intensive breaking in spite of the great steepness. As relative long wave travelling with short waves (wind waves) in the deep water, the experiment anticipates that the giant waves could appear based on BFI.

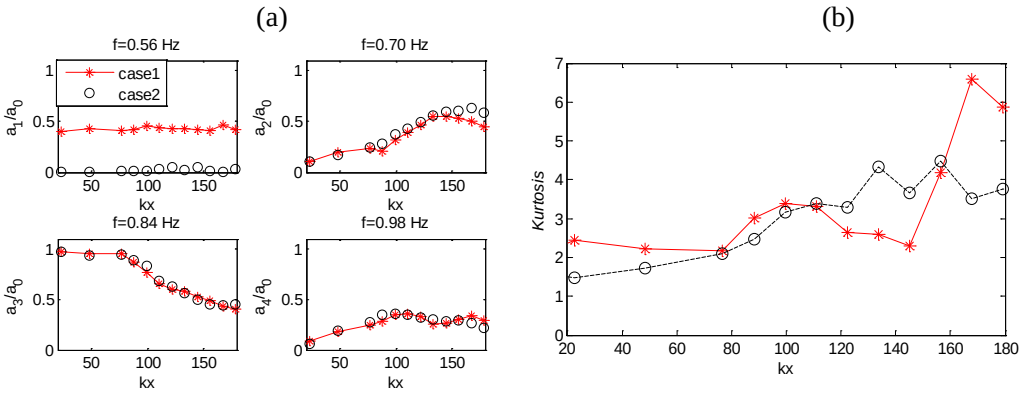

Figure 6. (a) Comparison of the spatial evolution of dimensionless amplitudes for Case 1 and Case 2 (b) and the kurtosis

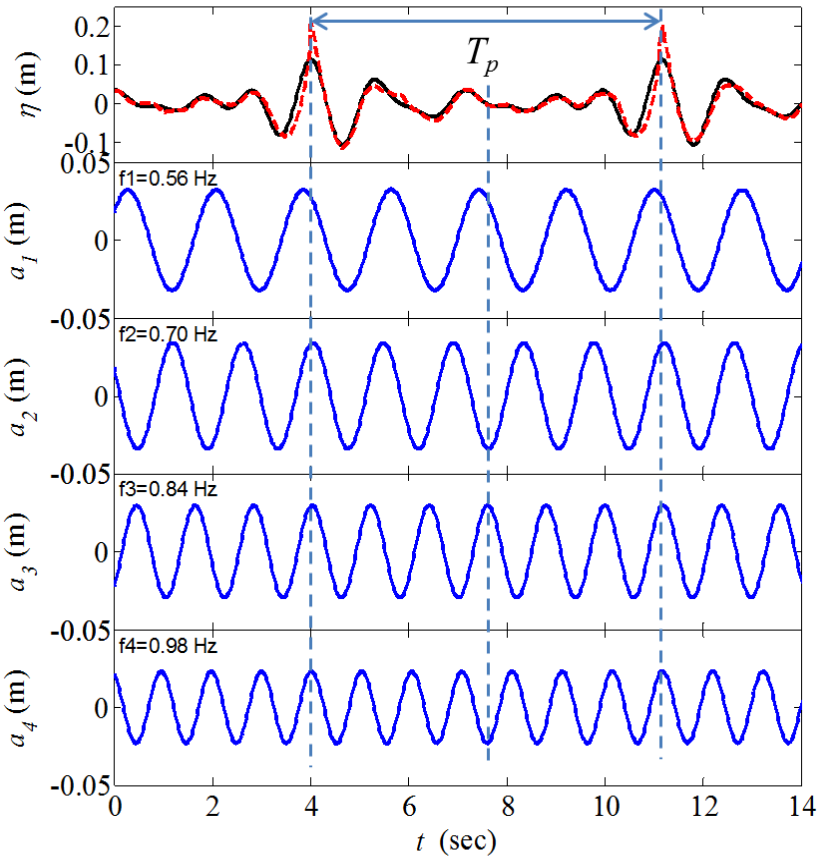

Figure 7. Top panel: Measured data, predicted signal from the superposition of four harmonics. Lower panels: time series of each harmonic from FFT.

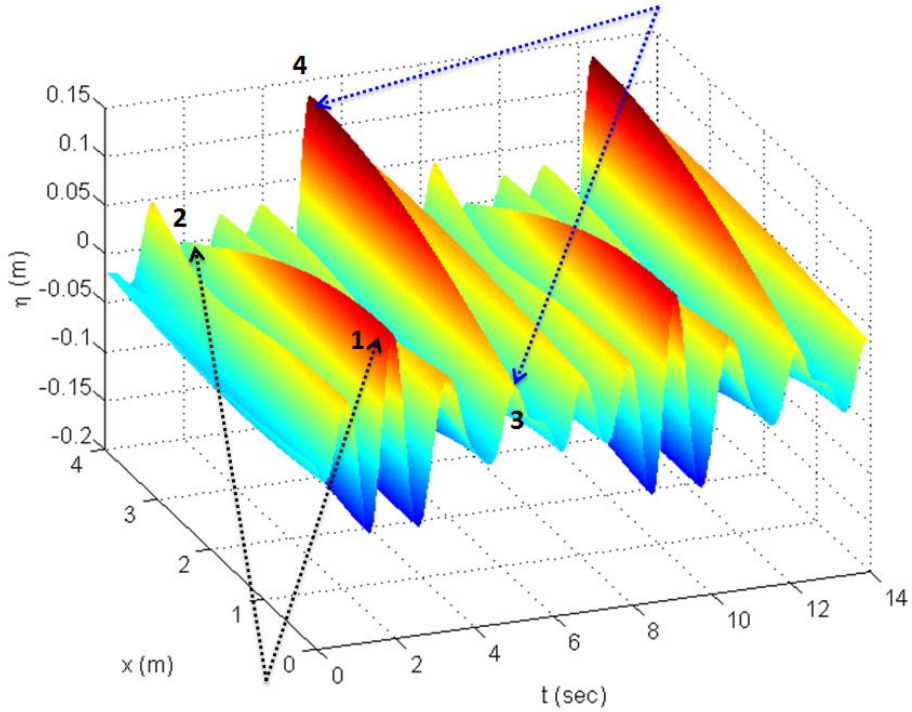

Figure 8. 3-D sketch of space and time series surface elevations from 10th to 11th

Conclusions

The nonlinear wave interactions within the frame work of BFI are investigated in this study. The discrete wave spectrum allow us to further analyze the kinematic and dynamic properties of every component in wave group such as variation of phase speeds and wave numbers. Higher frequency harmonics exhibit a much more strong nonlinear properties compare to long waves behavior. They are generally not well described either by the Stokes solution or resonant solutions. The wave breaking generally accompanies by the acceleration of the phase speed of every component, however, the modification for breaking is not considered in the present theories. On the other hand, the multiple nonlinear resonant interaction model generally has smaller discrepancies than Stokes solution. The local kurtosis strongly increases in the vicinity of large transient waves and can serve like a good indicator of extreme wave event.

Including the energy dissipation in the future would provide the more practical results. Finally, the relative long wave (storm wave) travelling with short waves (wind waves) in the deep water may play an important role for the generation of large transient wave and provide an opportunity for triggering the freak waves.

ACKNOWLEDGMENTS

The authors would like to thank the Ministry of Science and Technology of Taiwan (Grant supported by NSC 103-2911-I-006 -302) and the Aim for the Top University Project of National Cheng Kung University for their financial support.

REFERENCES

Benjamin, T. B. and J. E. Feir 1967. 'Disintegration of wave Trains on deep Water .1. Theory', *Journal of Fluid Mechanics* 27: 417

Banner, M. L., Barthelemy X., Fedele F., Allis M., Benetazzo A., Dias F. and Peirson, W. L. 2014. 'Linking Reduced Breaking Crest Speeds to Unsteady Nonlinear Water Wave Group Behavior', *Phys. Rev. Lett.*, 112 114502.

Chiang, W.-S. and H.-H. Hwung 2007. 'Steepness effect on modulation instability of the nonlinear wave train.' *Physics of Fluids* 19(1).

Grue, J., Clamond, D., Huseby, M., and Jensen, A., 2003 'Kinematics of extreme waves in deep water.' *Applied Ocean Research* 25(6): 355-366.

Galchenko A., Babanin A. V., Chalikov D., Young I.R., and Hsu T.W., 2010 'Modulational Instabilities and Breaking Strength for Deep-Water Wave Groups.' *J. Phys. Oceanogr.*, 40, 2313–2324.

Hwung, H. H., W. S. Chiang and S.C. Hsiao 2007. 'Observations on the evolution of wave modulation.' *Proceedings of the Royal Society*, 463(2077): 85-112.

Hwung, H.-H., Chiang W.-S., Yang, R.-Y. and Shugan, I. V. 2011 'Threshold Model on the Evolution of Stokes Wave Side-Band Instability.' *Eur. J. Mech. B/Fluids*, 30 147-155.

Janssen, P. 2003. 'Nonlinear four-wave interactions and freak waves.' *Journal of Physical Oceanography*, 33(4): 863-884.

Kharif, C. and E. Pelinovsky 2003. 'Physical mechanisms of the rogue wave phenomenon.' *European Journal of Mechanics B-Fluids* 22(6): 603-634.

Kartashova E., Shugan I. 2011. 'Dynamical cascade generation as a basic mechanism of Benjamin-Feir instability'. *Europian Physics Letters*. V.95, 30003.

Lake, B . M., Yuen,H . C., Rungaldiehr, and Ferqusown E. 1977 'Nonlinear deep-water waves: theory and experiment. Part 2. Evolution of a continuous wave train' *Journal of Fluid Mechanics* 83: 49-74

Longuet-Higgins MS 1975 'Integral properties of periodic gravity waves of finite amplitudes.' *Proc R Soc London* ,342:157–74.

Melville, W. K. 1983. 'Wave modulation and breakdown.' *Journal of Fluid Mechanics* 128: 489-506.

Phillips, O . M . 1977. The Dynamics of the Upper Ocean. Cambridge: Cambridge

Stansell P. and MacFarlane C., 2002 'Experimental Investigation of Wave Breaking Criteria Based on Wave Phase Speeds.' *J. Phys. Oceanogr*., 32, 1269–1283.

Tulin, M. P. and T. Waseda 1999. 'Laboratory observations of wave group evolution, including breaking effects.' *Journal of Fluid Mechanics* 378: 197-232.

Tamura, H., T. Waseda, and Y. Miyazawa 2009, 'Freakish sea state and swell-windsea coupling: Numerical study of the Suwa-Maru incident,' *Geophys. Res. Lett*., 36, L01607